



**Mauritius Research and Innovation Council**  
INNOVATION FOR TECHNOLOGY

**DESIGN CONSIDERATIONS FOR THE  
IMPLEMENTATION OF GREEN ROOFS  
IN MAURITIUS AND ANALYSIS OF  
IMPROVEMENT IN THERMAL  
COMFORT AND REDUCTION OF AIR-  
CONDITIONING ENERGY USING IN-  
SITU MEASUREMENT AND  
NUMERICAL ANALYSIS**

**Published Scientific Paper**

*April 2020*

**Mauritius Research and Innovation Council**

*Address:*  
Level 6, Ebene Heights  
34, Cybercity  
Ebene

Telephone: (230) 465 1235  
Fax: (230) 465 1239  
E-mail: [contact@mric.mu](mailto:contact@mric.mu)  
Website: [www.mric.mu](http://www.mric.mu)

**This scientific paper is based on work supported by the Mauritius Research and Innovation Council under award number MRC/RUN-1505. Any opinions, findings, recommendations and conclusions expressed herein are the author's and do not necessarily reflect those of the Council.**



# A numerical and experimental investigation of the effectiveness of green roofs in tropical environments: The case study of Mauritius in mid and late winter

Maheshsingh Mungur<sup>a</sup>, Yashna Poorun<sup>a</sup>, Diksha Juggurnath<sup>b</sup>, Yusra Bibi Ruhomally<sup>a</sup>, Reshma Rughooputh<sup>c</sup>, Muhammad Zaid Dauhoo<sup>a,\*</sup>, Abdel Khoodaruth<sup>b</sup>, Heman Shamachurn<sup>d</sup>, Mahendra Gooroochurn<sup>b</sup>, Navindra Boodia<sup>e</sup>, Mahindra Chooneea<sup>e</sup>, Sunita Facknath<sup>f</sup>

<sup>a</sup> Department of Mathematics, University of Mauritius, Mauritius

<sup>b</sup> Department of Mechanical and Production Engineering, University of Mauritius, Mauritius

<sup>c</sup> Department of Civil Engineering, University of Mauritius, Mauritius

<sup>d</sup> Department of Electrical and Electronic Engineering, University of Mauritius, Mauritius

<sup>e</sup> Department of Agricultural Production and Systems, University of Mauritius, Mauritius

<sup>f</sup> Department of Agriculture and Food Science, University of Mauritius, Mauritius

## ARTICLE INFO

### Article history:

Received 15 July 2019

Received in revised form

1 April 2020

Accepted 9 April 2020

Available online 28 April 2020

### Keywords:

Green roof

Heat and moisture transfer

Tropical climate

Conductive heat flux

Fourier transform

## ABSTRACT

The present work is a preliminary assessment of the performance of green roof at Reduit in Mauritius, located at latitude 20.23 °S and longitude 57.49 °E (Indian Ocean), which is influenced by a tropical humid climate. The efficiency of the green roof is gauged by evaluating its effect on indoor temperature fluctuations, conductive heat fluxes and the daily peak indoor temperature. On site measurements of weather data and indoor temperature are collected round the clock from July 11, 2017 to October 08, 2017. It is found that green roof increases the thermal mass of the experimental cells thereby reducing the fluctuations in indoor temperature. The conductive heat flux variation is significantly low in the case of the green roof. The green roof reduces the daily peak indoor temperature, which is attenuated significantly as compared to a conventional roof. A one dimensional mathematical model is also proposed in order to simulate the evolution of the heat and moisture transfer in a porous multilayer material. The model is validated using the measured data.

© 2020 Elsevier Ltd. All rights reserved.

## 1. Introduction

Green roofs are considered as one way to reduce the heat transfer into buildings. A green roof is a roof that is partially or completely covered with vegetation and a growing medium planted over a waterproofing membrane. It may also include additional layers such as a root barrier, drainage layer, filter cloth and irrigation systems. As stated in Berndtsson et al. [1], most of the researchers worldwide collectively agree that one way of reducing the impact of global warming and heat transfer into a building is the implementation of green roof technology. Green roof technology reduces energy consumption and improves internal comfort

during the spring and summer seasons in areas where the climate is characterized by high temperature and irradiance values during the day [2]. Several studies have proposed green roof models in the Northern hemisphere and highlighted the thermal contribution of vegetated roofs and their performance in reducing conductive heat flux in hot conditions ([3–5]). Amongst the studies conducted in the Southern hemisphere are the work due to Wong et al. [6], in which the authors performed experiments to assess the thermal benefits of a commercial building with a top roof garden. Closer to Mauritius, Dominique et al. [7] analysed the thermal and energetic behaviour of a green roof in Reunion island.

Various studies have emanated from the idea of modelling green roofs. Considerable work in terms of model development and analysis on green roof are elucidated below. More recently, in Ref. [8], the authors investigated on the variation of moisture

\* Corresponding author.

E-mail address: [m.dauhoo@uom.ac.mu](mailto:m.dauhoo@uom.ac.mu) (M.Z. Dauhoo).

content in a green roof. Additionally, a comparison of field observation with the simulations of the model is made using both a Reservoir Routing model and the Richards equation. Further, in Refs. [9], the thermal performance and the outdoor spatio-temporal performance of an extensive green roof are conducted. Different weather scenarios were analysed and it was observed that sunny days have the highest impact on the thermal performance which have a less pronounced effect on cloudy and rainy days.

Several mathematical models have been formulated for the green roof which cater for different aspects. In this work [10], the authors model the heat transfer for a green roof by taking into account the heterogeneity of some of the layers in it. Ouldboukhithine et al. [11] proposed a model based on energy balance equations expressed for foliage and soil media. The simulation results showed that the use of vegetation on the roof building improves not only the thermal comfort conditions, but also the energy performance of a building. In Rakotondramiarana et al. [12], a hygrothermal green roof model with a thermal model to evaluate the energy performance and thermal comfort of the building is developed. The model was used to assess the impact on indoor air temperature and energy demand in Madagascar. In Sailor [13], a physically based model of the energy balance of a green roof has been developed and integrated into the EnergyPlus building energy simulation program. The model is based on heat and moisture exchange process above vegetated soil. Many studies have recently been conducted to improve the thermal performance of green roofs ([14–19]).

Some studies [20–22] show that green roofs can bring energy saving in buildings. Leonard [23] shows that green roofs suppress the downward heat flux into the top-floor indoor area to reduce air conditioning electricity consumption. Due to the high heat recorded in Mauritius in December 2019, a significant increase has been noted in the demand for electricity, with a peak of around 507.2 MW [24]. Electricity consumption is higher than normal, especially with the use of air conditioners and fans. In Elahee [25], it is highlighted that air conditioning is generally reckoned to account for between 30% and 50% of electricity consumption in buildings in Mauritius while the rest being mostly due to lighting, refrigeration and other electrical appliances. Moreover, in Adam Badurally [26], it is stressed that in Mauritius, the peak electricity demand will continuously rise over the years. Furthermore, using genetic algorithm, the authors in Ref. [26] found that the monthly mean temperature is highly correlated to maximum power demand thereby confirming the impact of high temperatures. Hence, this explains the massive use of air conditioning in Mauritius. Accordingly, a remedy to this situation is essential and an alternative to the use of air conditioners is needed.

The impact of climatic conditions on the efficacy of green roofs has been studied in Ref. [27–29] and it has been shown that climate affects the performance of green roofs. In general, the roof of a building receives the maximum solar radiation as compared to the vertical walls, thereby causing excessive heat flow in the room [30]. Further, it is known that 50% of a building's cooling load originates from the roof [5,10,30]. It is therefore essential to gauge the effect of green roofs in the context of the Mauritian climate.

In the present work, the factors measured in order to analyse the efficiency of green roof are the temporal evolution of the following weather parameters: i) outdoor temperature, ii) solar radiation, iii) rainfall and iv) the peak daily indoor temperature. Using the above measured data, the evolution of the conductive heat flux is evaluated. Then, the daily peaks in indoor temperature and the time at which these occur are identified from the power spectrum of the variation of the indoor temperature, using Discrete Fourier Transform. In order to assess the efficiency of a green roof in different seasons in Mauritius, experiments can be conducted and measurements can be recorded for a year long period. In addition, it

should be noted that anomalies due to experimental setups and measurements have to be taken into account. Therefore, the availability of a reliable mathematical model on the dynamics of heat and moisture transfer will enable us to gain time and overcome the above mentioned drawbacks. Also, if a model is verified and validated as proposed in the current work, a quite accurate estimation of important parameters such as the indoor temperature can be obtained. Moreover, numerous scenario analysis can be effectuated by varying the different parameters involved. Thus, for example, if the planting material property is adjusted accordingly in the Table 2 and the data feed to the model, the green roof can be tested for different plants. In this sense, a verified and validated mathematical model can be very versatile and practical to carry out experimental studies.

The paper is organized as follows: section 2 describes the green roof system while section 3 presents the heat and moisture transfer in the green roof model. Sections 4 and 5 present the weather data and describe the experimental setup in Mauritius. Section 6 presents an analysis of the experimental and numerical results obtained from measured data and the mathematical model respectively. A comparison of the thermal performance of the green roof and conventional roof is also conducted. The concluding remarks are eventually provided in section 7.

## 2. System description

The experiments with the green roof are conducted from July 11, 2017 to October 08, 2017. The cells involved in the experiment are located at Reduit, Mauritius (latitude 20.23 °S and longitude 57.49 °E) which is 303.6 m above sea level. Mauritius is characterized by two seasons namely, winter and summer. The daily average temperature of ambient air is 20.4 °C and 24.7 °C respectively [31]. Mauritius benefits of abundant solar radiation throughout the year and this can be seen in Fig. 1. The green roof cell in the present experiment is composed of concrete, waterproofing membrane, a layer of soil, a drainage layer and its vegetation as shown in Fig. 2.

Information on the depth of each component is given in Table 1.

The values given in Table 2 are adopted for the different materials.

The bulk density of the substrate is measured experimentally by taking a 3-inch diameter ring in each cell containing Bulbine and Rhoeo plants. The bulk density of the substrate containing Bulbine and Rhoeo is given by 0.134 and 0.104 respectively. The water holding capacity and the porosity of the substrate containing Bulbine are 0.8696 and 0.863 respectively, whereas for Rhoeo, it is 0.877 and 0.8753 respectively.

## 3. Mathematical model

A one dimensional heat and moisture transfer mathematical model is developed for the green roof model. The system is composed of four different layers as shown in Fig. 2. The assumptions are as follows: (i) convective heat and convective mass transfer are not modelled, (ii) vapour-phase transport is only with vapour diffusion and solution diffusion, (iii) liquid phase water transport is only with capillary and surface diffusion, (iv) vapour diffusivity, suction pressure, air permeability and hysteresis in sorption isotherm are neglected, (v) in the outside boundary condition, we neglect air pressure and water leakage, (vi) in the inside boundary condition, we neglect air pressure and interior stack effect. The system of partial differential equations (PDEs) for the heat and moisture transfer is given by the moisture balance eq (1) and heat balance eq (2).

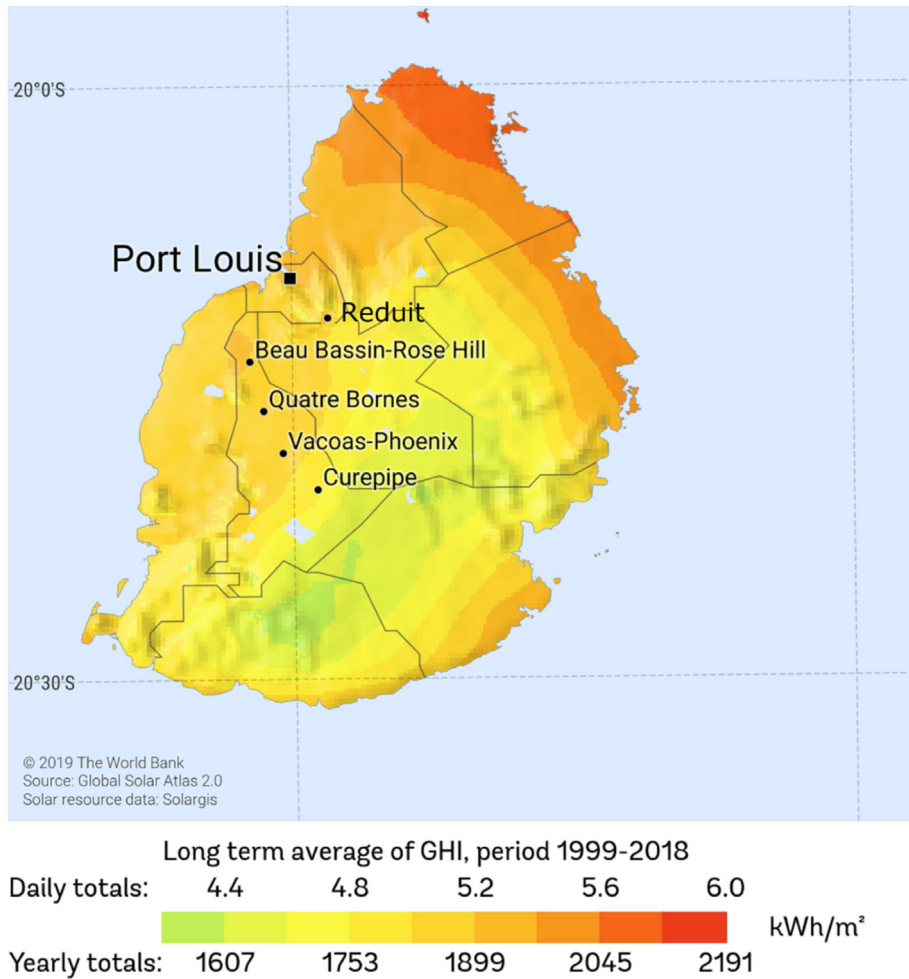


Fig. 1. Global Horizontal Irradiance distribution in Mauritius during the period 1999–2018 [32].

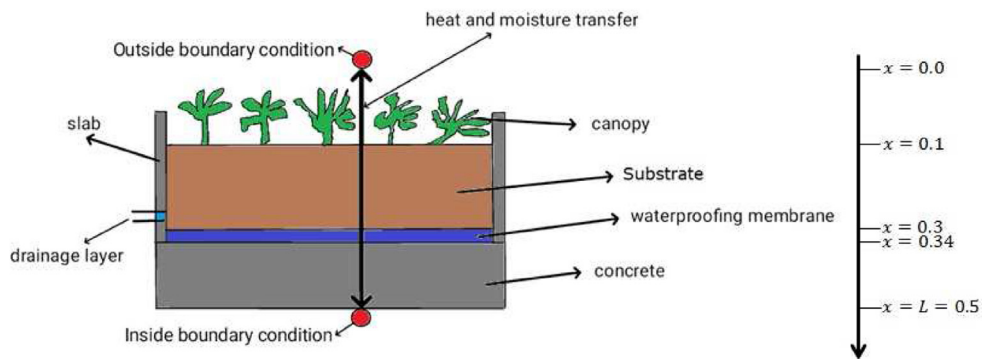


Fig. 2. Structural composition of the green roof under consideration. (For interpretation of the references to colour in this figure legend, the reader is referred to the Web version of this article.)

**Table 1**  
Depth of materials present in the green roof.

Material	Depth
Concrete	15 cm
Waterproofing membrane	0.4 cm
Layer of soil	20 cm
Vegetation	varies between 10 cm and 20 cm depending on the type of plants used.

**Table 2**  
Material properties of the layers in the green roof.

	$\rho_B(\text{kg}/\text{m}^3)$	$P(\text{m}^3/\text{m}^3)$	$c_s(J/(kgK))$	$\lambda(W/(mK))$	$\mu$
Concrete C25	2450	0.15	800	1.6	248
Waterproofing membrane substrate	1000	0.0002	1500	0.16	40000
	134	0.863	2600	0.048	31
Planting	1500	0.5	1000	0.2	5

$$\frac{\partial w}{\partial t} + \nabla \cdot g = S_w \tag{1}$$

and

$$\frac{\partial H}{\partial t} + \nabla \cdot q = S_h \tag{2}$$

In the differential eq (2), phase change is given by the source term

$$S_h = h_v \nabla \cdot g_v \tag{3}$$

The saturation pressure can be approximated using the function

$$P_{sat} = 611 \cdot \exp\left(\frac{b \cdot T}{\vartheta_0 + T}\right) \tag{4}$$

where

$$\begin{aligned} b &= 22.44 & \vartheta_0 &= 272.44^\circ\text{C} & \text{if } T < 0^\circ\text{C} \\ b &= 17.08 & \vartheta_0 &= 234.18^\circ\text{C} & \text{else } T \geq 0^\circ\text{C} \end{aligned} \tag{5}$$

The vapour flux,  $g_v$ , and the liquid flux,  $g_l$ , are given by

$$g_v = -\delta_p \nabla p_v \tag{6}$$

and

$$g_l = -D_h \nabla h \tag{7}$$

The heat content is expressed as

$$H = H_s + H_w \tag{8}$$

where

$$H_s = \rho_B c_s T \tag{9}$$

and

$$H_w = (w - w_e)c_w + w_e c_e - h_e \frac{dw_e}{dT} \tag{10}$$

Thus, the moisture balance and heat balance equations are simplified as

$$\frac{\partial w}{\partial t} = \nabla(D_h \nabla h + \delta_p \nabla(p_v)) \tag{11}$$

and

$$\frac{\partial H}{\partial t} = \nabla(\lambda \nabla T) + h_v \nabla(\delta_p \nabla(p_v)) \tag{12}$$

[33].

Since  $w$  and  $H$  are functions of  $h$  and  $T$  respectively, eqs (11) and (12) can be written as

$$\frac{dw}{dh} \frac{\partial h}{\partial t} = \nabla \cdot \left( (D_h + \delta_p P_{sat}) \nabla h + \delta_p h \frac{dP_{sat}}{dT} \nabla T \right) \tag{13}$$

and

$$\frac{dH}{dT} \frac{\partial T}{\partial t} = \nabla \cdot \left( \left( \lambda + h_v \delta_p h \frac{dP_{sat}}{dT} \right) \nabla T + h_v \delta_p P_{sat} \nabla h \right) \tag{14}$$

Next, the well-posedness of eqs (13) and (14) is established. One important aspect of the mathematical model is that the system of eqs (13) and (14), together with the boundary condition in eqs (15) and (16), must have a unique solution. That is, for each initial condition, there exists one and only one corresponding solution. In this case, the system of eqs (13) and (14) is said to be well-posed and thus can be solved numerically. In the appendix, the problem given by eqs (13) and (14) is proved to be well-posed under certain conditions which are implemented when computing the solution.

### 3.1. Numerical discretization

The one dimensional heat and moisture transfer equations given by eq (11) and eq (12) are rewritten as

$$\frac{dw}{dh} \frac{\partial h}{\partial t} = \frac{\partial}{\partial x} \left( D_h \frac{\partial h}{\partial x} \right) + \frac{\partial}{\partial x} \left( \delta_p \frac{\partial}{\partial x} (h P_{sat}) \right) \tag{15}$$

and

$$\frac{dH}{dT} \frac{\partial T}{\partial t} = \frac{\partial}{\partial x} \left( \lambda \frac{\partial T}{\partial x} \right) + h_v \frac{\partial}{\partial x} \left( \delta_p \frac{\partial}{\partial x} (h P_{sat}) \right) \tag{16}$$

An implicit FDM is used to approximate eqs (15) and (16) numerically. Implicit schemes are known to produce physically realistic approximations with larger time steps. The spatial and temporal domains comprise of  $J$  intervals of step length  $\Delta x = L/(J - 1)$  and  $N$  intervals of step length  $\Delta t$ . Let  $x_j = j \Delta x$  for  $j = 1, \dots, J$  and  $t_n = n \Delta t$  for  $n = 1, \dots, N$  and  $t > 0$ , respectively. The discrete variables for temperature and moisture,  $T_j^n$  and  $h_j^n$  respectively, are given by

$$\begin{aligned} \frac{1}{\Delta t} \left( \frac{dH}{dT} \right)_j (T_j^{n+1} - T_j^n) &= \frac{1}{(\Delta x)^2} \left( \lambda_{j+1}^n (T_{j+1}^{n+1} - T_j^{n+1}) - \lambda_j^n (T_j^{n+1} - T_{j-1}^{n+1}) \right) + \frac{h_v}{(\Delta x)^2} \left( \delta_{p,j+1}^n \left( h_{j+1}^n \frac{\partial P_{sat}}{\partial T} \Big|_{T=T_{j+1}^n} (T_{j+1}^{n+1} - T_{j+1}^n) \right) \right. \\ &\quad \left. + h_{j+1}^n P_{sat,j+1}^n - h_j^n \frac{\partial P_{sat}}{\partial T} \Big|_{T=T_j^n} (T_j^{n+1} - T_j^n) - h_j^n P_{sat,j}^n \right) + h_j^n P_{sat,j}^n - h_{j-1}^n \frac{\partial P_{sat}}{\partial T} \Big|_{T=T_{j-1}^n} (T_{j-1}^{n+1} - T_{j-1}^n) - h_{j-1}^n P_{sat,j-1}^n \end{aligned} \tag{17}$$

and

$$\frac{1}{\Delta t} \left( \frac{dw}{dh} \right)_j^n (h_j^{n+1} - h_j^n) = \frac{1}{(\Delta x)^2} \left( D_{h,j+1}^n (h_{j+1}^{n+1} - h_j^{n+1}) - D_{h,j}^n (h_j^{n+1} - h_{j-1}^{n+1}) \right) + \frac{1}{(\Delta x)^2} \left( \delta_{p,j+1}^n (h_{j+1}^{n+1} P_{sat,j+1}^{n+1} - h_j^{n+1} P_{sat,j}^{n+1}) - \delta_{p,j}^n (h_j^{n+1} P_{sat,j}^{n+1} - h_{j-1}^{n+1} P_{sat,j-1}^{n+1}) \right),$$

respectively, for  $j = 2, \dots, J - 1$ , where the time level  $n$  is known and  $n + 1$  is unknown. The moisture and radiative exchanges between soil and canopy layer are taken into account in the form of heat source and moisture source terms which are added to eqs (15) and (16) respectively. In the present context, the heat source term  $S_H$  is approximated by a fraction of solar radiation. Thus, it is given by

$$S_H = (1 - \sigma_c)I, \tag{18}$$

where  $\sigma_c$  is the fractional vegetation coverage. In the experiments, the greenroof soil is covered by 50%–80% of vegetation. Hence, as an approximation, we take  $\sigma_c = 0.7$ . The moisture source term  $S_w$  is given by a fraction of driving rain [34] as

$$S_w = (1 - \sigma_c)R_s. \tag{19}$$

At the interface between the soil and canopy at,  $x = 0.1$ , the discretized equations are given by

$$\frac{1}{\Delta t} \left( \frac{dH}{dT} \right)_j^n (T_j^{n+1} - T_j^n) = \frac{1}{(\Delta x)^2} \left( \lambda_{j+1}^n (T_{j+1}^{n+1} - T_j^{n+1}) - \lambda_j^n (T_j^{n+1} - T_{j-1}^{n+1}) \right) + \frac{h_v}{(\Delta x)^2} \left( \delta_{p,j+1}^n \left( h_{j+1}^n \frac{\partial P_{sat}}{\partial T} \Big|_{T=T_{j+1}^n} (T_{j+1}^{n+1} - T_{j+1}^n) + h_{j+1}^n P_{sat,j+1}^n - h_j^n \frac{\partial P_{sat}}{\partial T} \Big|_{T=T_j^n} (T_j^{n+1} - T_j^n) - h_j^n P_{sat,j}^n \right) + h_j^n P_{sat,j}^n - h_{j-1}^n \frac{\partial P_{sat}}{\partial T} \Big|_{T=T_{j-1}^n} (T_{j-1}^{n+1} - T_{j-1}^n) - h_{j-1}^n P_{sat,j-1}^n \right) \tag{20}$$

and,

$$\frac{1}{\Delta t} \left( \frac{dw}{dh} \right)_j^n (h_j^{n+1} - h_j^n) = \frac{1}{(\Delta x)^2} \left( D_{h,j+1}^n (h_{j+1}^{n+1} - h_j^{n+1}) - D_{h,j}^n (h_j^{n+1} - h_{j-1}^{n+1}) \right) + \frac{1}{(\Delta x)^2} \left( \delta_{p,j+1}^n (h_{j+1}^{n+1} P_{sat,j+1}^{n+1} - h_j^{n+1} P_{sat,j}^{n+1}) - \delta_{p,j}^n (h_j^{n+1} P_{sat,j}^{n+1} - h_{j-1}^{n+1} P_{sat,j-1}^{n+1}) \right) + S_w. \text{The discrete boundary conditions at } x = 0 \text{ are given as,}$$

$$\frac{1}{\Delta t} \left( \frac{dH}{dT} \right)_1^n (T_1^{n+1} - T_1^n) = \frac{1}{(\Delta x)^2} \lambda_2^n (T_2^{n+1} - T_1^{n+1}) + \frac{h_v}{(\Delta x)^2} \delta_{p,2}^n \left( h_2^n \frac{\partial P_{sat}}{\partial T} \Big|_{T=T_2^n} (T_2^{n+1} - T_2^n) + h_2^n P_{sat,2}^n - h_1^n \frac{\partial P_{sat}}{\partial T} \Big|_{T=T_1^n} (T_1^{n+1} - T_1^n) - h_1^n P_{sat,1}^n \right)$$

and

$$\frac{1}{\Delta t} \left( \frac{dw}{dh} \right)_1^n (h_1^{n+1} - h_1^n) = \frac{1}{(\Delta x)^2} D_{h,2}^n (h_2^{n+1} - h_1^{n+1}) + \frac{1}{(\Delta x)^2} \delta_{p,2}^n (h_2^{n+1} P_{sat,2}^{n+1} - h_1^{n+1} P_{sat,1}^{n+1}) - \frac{1}{\Delta x} (a_r R_N$$

$$+ \beta (h_1^{n+1} P_{sat,1}^{n+1} - p_a)).$$

Analogously, at  $x = L$

$$\frac{1}{\Delta t} \left( \frac{dH}{dT} \right)_J^n (T_J^{n+1} - T_J^n) = -\frac{1}{(\Delta x)^2} \lambda_J^n (T_J^{n+1} - T_J^{n+1}) - \frac{h_v}{(\Delta x)^2} \delta_{p,J}^n \left( h_J^n \frac{\partial P_{sat}}{\partial T} \Big|_{T=T_J^n} (T_J^{n+1} - T_J^n) + h_J^n P_{sat,J}^n - h_{J-1}^n \frac{\partial P_{sat}}{\partial T} \Big|_{T=T_{J-1}^n} (T_{J-1}^{n+1} - T_{J-1}^n) - h_{J-1}^n P_{sat,J-1}^n \right)$$

and

$$\frac{1}{\Delta t} \left( \frac{dw}{dh} \right)_J^n (h_J^{n+1} - h_J^n) = -\frac{1}{(\Delta x)^2} D_{h,J}^n (h_J^{n+1} - h_{J-1}^{n+1}) - \frac{1}{(\Delta x)^2} \delta_{p,J}^n (h_J^{n+1} P_{sat,J}^{n+1} - h_{J-1}^{n+1} P_{sat,J-1}^{n+1}) + \frac{1}{\Delta x} \beta (p_s - h_J^{n+1} P_{sat,J}^{n+1}).$$

At each time step, a tridiagonal solver is used to obtain the updated heat and moisture components.

### 3.2. Boundary conditions

Important exterior environmental parameters, namely, ambient temperature and solar radiation, influence the heat and moisture transfer in the green roof. Therefore, these parameters are taken into account at the boundary conditions of the model. At the outer boundary ( $x = 0$ ), the mass and heat fluxes are given by:

$$q_h = \beta(p_v - p_a) + a_r R_N \quad q_T = \alpha(T - T^*) \tag{21}$$

respectively, where  $p_a$  is the water vapour pressure in the ambient air. The equivalent ambient temperature,  $T^*$ , incorporates the effect of solar radiation on the temperature of the exterior surface.

$$T^* = T_a + I/\alpha_c,$$

where  $\alpha = \alpha_c + \alpha_r$ . The convective heat transfer coefficient  $\alpha_c$  for the green roof is a function of wind velocity based on an experimental study [35].

$$\alpha_c = 14.384 + 6.8007v + 4.5474v^2 - 1.391v^3 \tag{22}$$

and  $\alpha_r$  is taken as 6.5. The net solar radiation to the exterior surface,  $I$ , is calculated as

$$I = aI_s + \varepsilon I_l - I_e. \tag{23}$$

The radiation balance in the thermal domain  $\varepsilon I_l - I_e$  usually has a lower value than  $aI_s$  but it is the only component at night as  $I_s$  will be zero.  $I_l$  and  $I_e$  can be expressed as a function of air temperature and canopy surface temperature

$$I_l = \varepsilon_a \sigma T_a^4 \text{ and } I_e = \varepsilon \sigma T_s^4 \tag{24}$$

where  $\varepsilon_a$  is the emissivity of the atmosphere and  $\varepsilon$  is the emissivity of the canopy [36].

Also, at the inner surface ( $x = L$ ), the following mass and heat fluxes are assumed:

$$q_h = \beta(p_s - p_v) \text{ and } q_T = \alpha(T_s - T) \tag{25}$$

respectively, where  $p_s$  is the water vapour pressure of the roof's surface. Therefore, the PDEs governing the boundary conditions for

moisture and temperature are

$$D_h \frac{\partial h}{\partial x} + \delta_p \frac{\partial}{\partial x} (hP_{sat}) = q_h \quad (26)$$

and

$$\lambda \frac{\partial T}{\partial x} + h_v \delta_p \frac{\partial}{\partial x} (hP_{sat}) = q_T \quad (27)$$

respectively.

Simulations are run with the above described model using weather data measured at Reudit.

#### 4. Weather data

The data has been recorded from 11 July to October 08, 2017. The mid winter season is from 11 July to August 08, 2017 and the late winter season is from 10 September to October 08, 2017. The ambient temperature, solar radiation, atmospheric pressure and rain are the weather data input to the mathematical model. We use a Davis Vantage Pro 2 Weather Station to collect weather data. The following environmental parameters, namely: (i) solar radiation ( $W/m^2$ ), (ii) ambient temperature ( $^{\circ}C$ ) and (iii) rainfall ( $mm$ ), have been recorded in mid winter and late winter. These parameters shown in Figs. 3, 4 and 5 respectively, are used in the green roof model.

In the section that follows, we describe the experimental setup used in order to explore the green roof potential through the determination of its effect on indoor temperature fluctuations, conductive heat flux and daily peak indoor temperatures.

#### 5. Experimental setup

Fig. 6 shows the green roof cells at the University of Mauritius. The experimental model comprises of 9 identical cells of exterior dimension of  $156 \text{ cm} \times 141 \text{ cm} \times 122 \text{ cm}$  and a facade of height 34 cm above the roof, as illustrated in Fig. 7.

Each green roof cell is composed of concrete, waterproofing

membrane, a layer of soil, waterproofing paint, a drainage layer and its vegetation.

Three cells contain Bulbine plants, three contain Rhoeo plants and the remaining cells have no plant or substrate. Each cell has a planting area of 135 cm by 105 cm in which 13 plants are planted.

The substrate used in the green roof is made up of 20% compost and 80% coconut coir. The compost is mixed manually with coir (coming from an established greenhouse hydroponic business) until a homogeneous mixture is obtained [37]. Coir products are chosen because they provide a range of water-holding and air-filled space by mixing different particle sizes and ratios together. Bulbine and Rhoeo plants are chosen because they are drought tolerant and grow well in poor soils. These plants tolerate summer heat well and any type of garden soil provided the substrate is well drained [38].

Different instruments are used to record temperature and moisture content in the experimental model. A HOBO 4-channel Thermocouple Data Logger UX120-014 M is used to record temperature inside and outside the cell. We use a thermocouple of type J which has a range of  $-20^{\circ}C$  to  $70^{\circ}C$  with an accuracy of  $\pm 0.21^{\circ}C$  from  $0^{\circ}$  to  $50^{\circ}C$  accuracy and resolution of  $0.024^{\circ}C$ . A calibration of 4 thermocouple thermometers at Mauritius Standard Bureau (MSB) is done using the 580 OCEANUS-6 calibration laboratory and the Heto HPT550 Precision thermometer. Each data logger records the temperature inside and outside the cell at 1 min intervals. We have collected data for almost 5 months for the 9 cells. In each cell, two sensors are placed on the ceiling of the cell (inside) and this can be seen in Fig. 8. The instruments used to record the temperature inside the cell are shown in Fig. 9.

In the section that tails, the numerical results of the green roof and that of the mathematical model are presented.

#### 6. Results and discussion

##### 6.1. Comparison of experimental results between green roof and conventional roof

The variation of the mean indoor surface temperature for the cells with a green roof consisting of Bulbine (cell 1, cell 5 and cell 9) and cells with Rhoeo (cell 2, cell 6 and cell 7) respectively, is shown

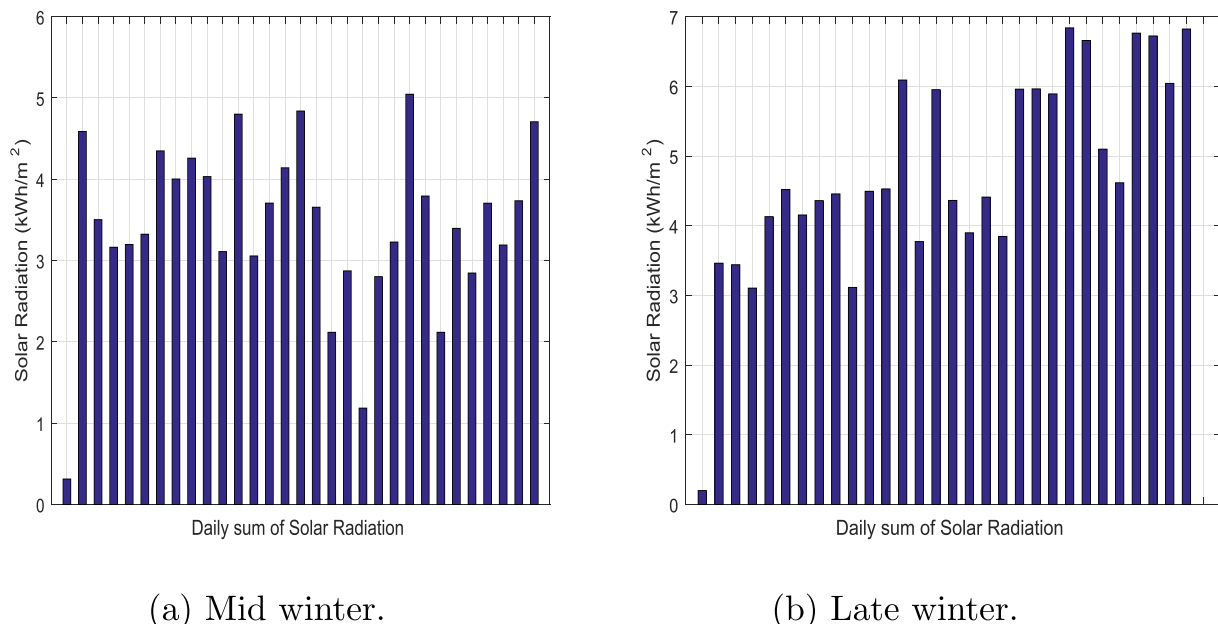
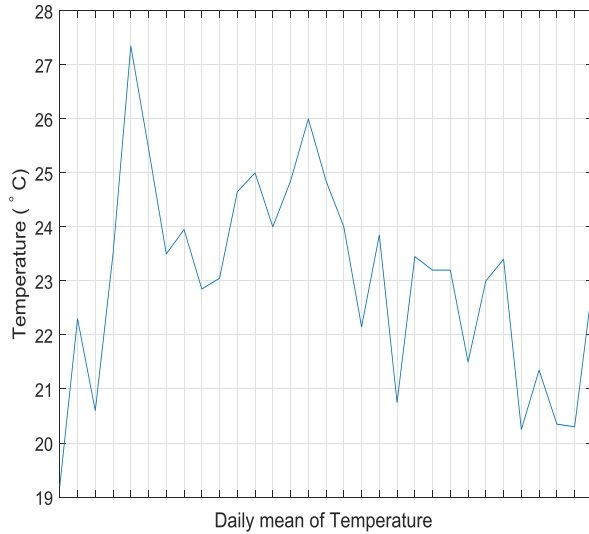
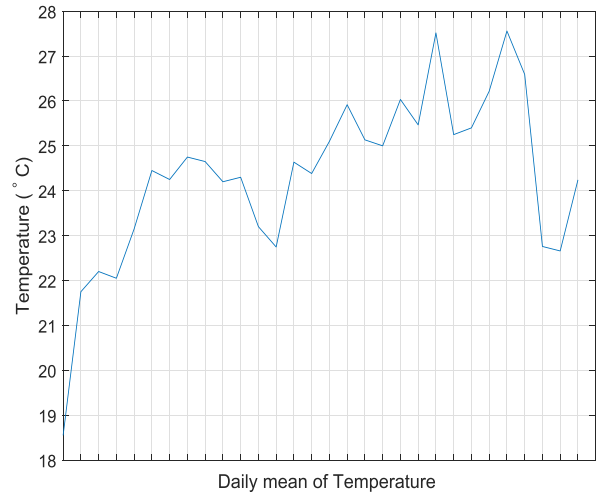


Fig. 3. The temporal evolution of solar radiation.

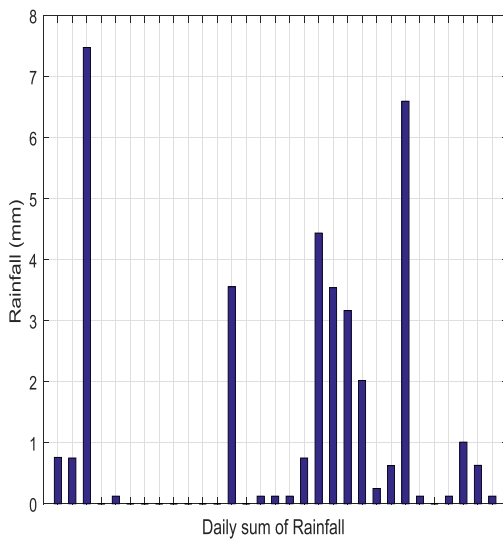


(a) Mid winter.

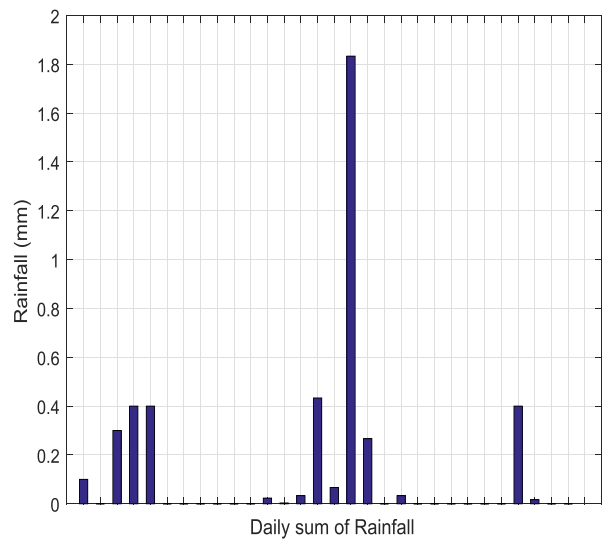


(b) Late winter.

Fig. 4. The temporal evolution of ambient temperature.



(a) Mid winter.



(b) Late winter.

Fig. 5. The temporal evolution of rainfall.

in Fig. 10.

It can be observed from Fig. 10 that the difference in the indoor temperature measured round the clock for the period of mid winter is negligible. In this sense, for the sake of simplicity, we choose only one cell for the following numerical experiments and analyses. Next, we compare the outside air temperature and indoor surface temperature for a green roof cell and a conventional roof in mid winter and late winter.

Figs. 11 and 12 show that the inside temperature fluctuates less for the green roof in both mid winter and late winter. It is observed that the indoor roof temperature of a green roof decreases by a maximum of 3 °C in mid winter and 4 °C in late winter as compared to the ambient temperature. However, a significant

reduction in temperature is observed in the indoor roof surface temperature of a green roof as compared to that of a conventional roof. There is clear evidence that the green roof provides better thermal performance than a conventional roof in the sense that it stabilises the temperature.

### 6.1.1. Frequency domain of the temperature data

We use the Fourier transform to analyse the temperature data for the green roof and conventional roof in mid winter and late winter. The Fourier transform helps to decompose the temperature series into corresponding components of sinusoidal waves, thus transforming the time domain to a frequency domain using the Discrete Fourier Transform (DFT) tool.



Fig. 6. The 6 green roof cells. (For interpretation of the references to colour in this figure legend, the reader is referred to the Web version of this article.)

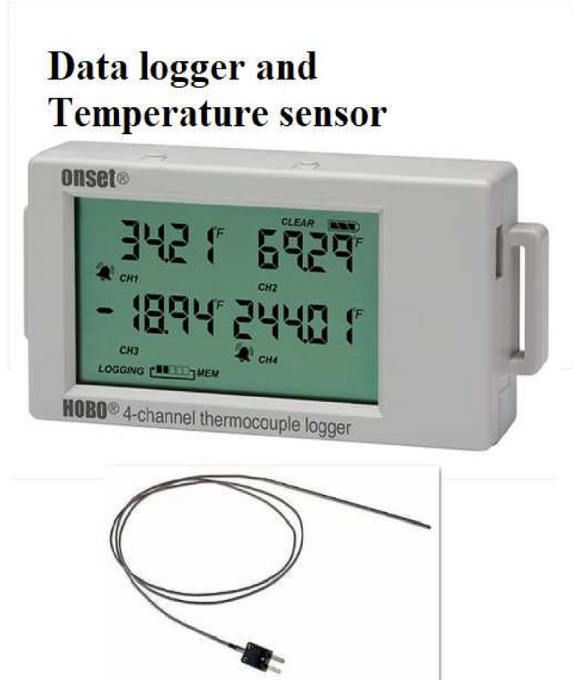


Fig. 9. Data logger and thermocouple used to record temperature inside the cell.

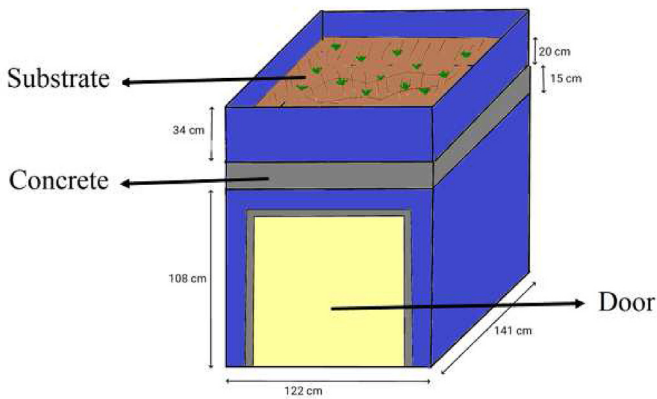


Fig. 7. Dimension of green roof cell. (For interpretation of the references to colour in this figure legend, the reader is referred to the Web version of this article.)

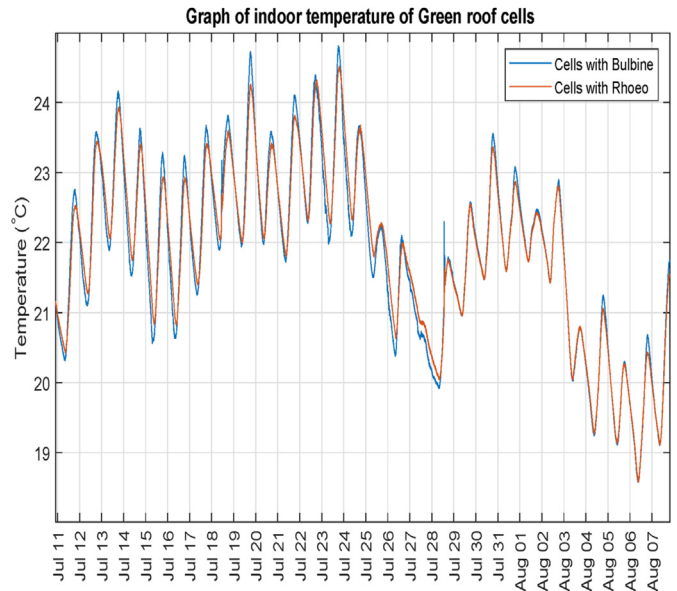


Fig. 10. Comparing the indoor temperature of cells with green roof in mid winter. (For interpretation of the references to colour in this figure legend, the reader is referred to the Web version of this article.)

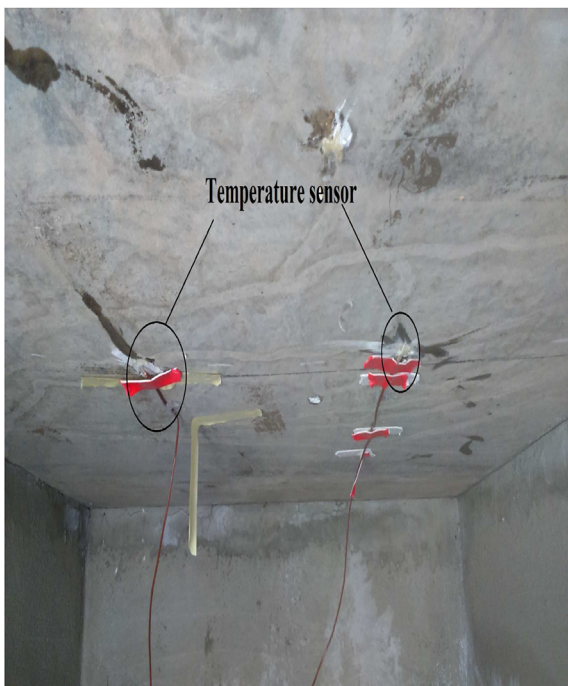
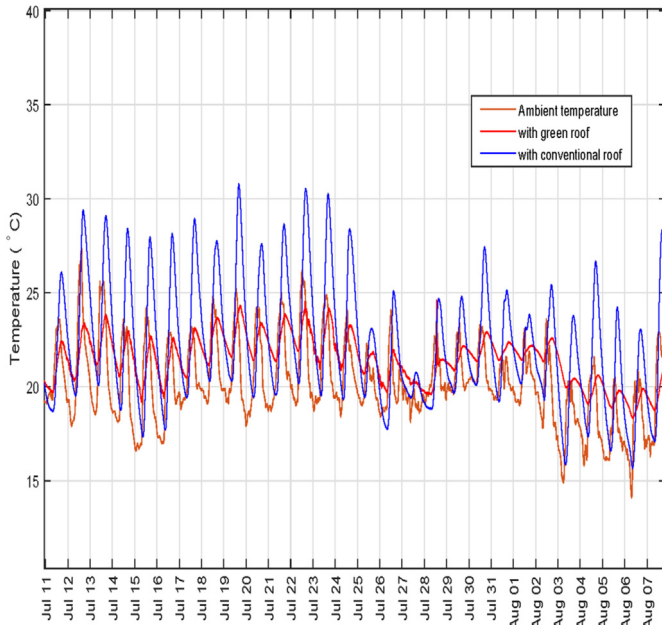


Fig. 8. Location of the temperature sensor inside the cell.

Consider a set of data  $\{x(n)\}_{n=0}^{N-1}$ . The DFT of the data is given by a sequence  $X(k), k = 0, \dots, N - 1$ , where

$$X(k) = \sum_{n=0}^{N-1} x(n) \exp^{-2\pi i \frac{nk}{N}}, \quad (28)$$

where  $N$  is the total number of collected data and  $i$  is the unity imaginary number ( $i = \sqrt{-1}$ ). An efficient way of computing the DFT is by using the Fast Fourier Transform (FFT). The MATLAB



**Fig. 11.** Variation of outside air temperature and indoor surface temperature for a green roof cell and a conventional roof respectively in mid winter. (For interpretation of the references to colour in this figure legend, the reader is referred to the Web version of this article.)

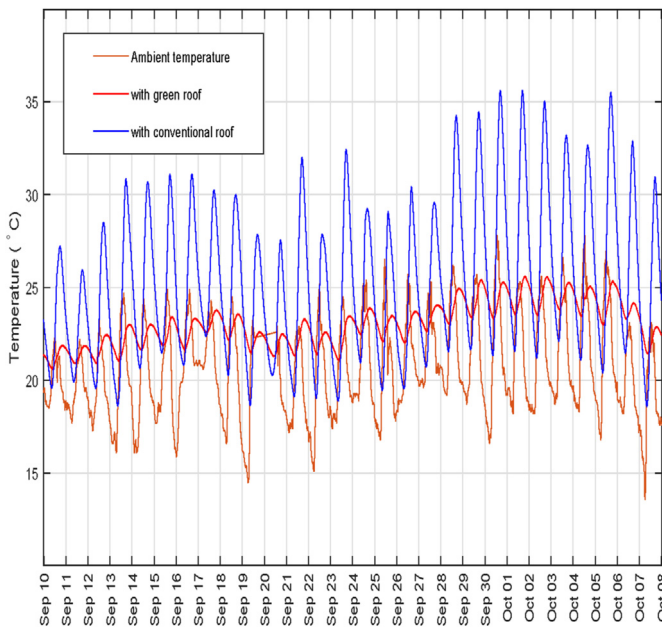


**Fig. 12.** Variation of outside air temperature and indoor surface temperature for a green roof cell and a conventional roof respectively in late winter. (For interpretation of the references to colour in this figure legend, the reader is referred to the Web version of this article.)

function  $fft$  is used to calculate the DFT in this work. The vector,  $X(k)$ , is complex valued and the strength of the variation of the data is expressed by a real value Power Spectral Density given by

$$S(k) = \frac{1}{N} |X(k)|^2. \tag{29}$$

The frequency domain reveals periodicities in the input data and

the relative strength of the periodic component. Next, we use the Fourier transform to analyse the temperature data for the green roof and conventional roof. We plot the power spectrum of the temperature data of green roof and conventional roof in Fig. 13a and b respectively.

The large DC component at frequency zero gives the mean of the temperature data and does not contain any information about the periodicity of the data [39]. From Fig. 13b and a, it is seen that a large peak occurs once during one day for both the green roof and conventional roof. This variation is known as the diurnal temperature which relates to the difference between a high temperature and a low temperature that occurs during the same day. The amplitude of the power spectrum in  $^\circ\text{C}$  shows the change of temperature from its mean during one day. For the green roof, the peak occurs at  $0.87^\circ\text{C}$  whereas for the conventional roof it occurs at  $3.6^\circ\text{C}$ . The green roof contributes to the modification of the decrement factor of the constituent material of the roof, thereby stabilizing the temperature. Since the decrement factor regulates the conductive heat flux, a peak with a lower amplitude is seen in the case of the green roof, which means that fluctuations in temperature are reduced. It is also observed that the peak ambient temperature occurs at midday. However, the peak indoor temperature of both green roof and conventional roof occurs late in the afternoon. This is because of the decrement factor of the building material of the roof which stores the amount of heat and later on releases it from inside. Therefore, this contributes to the increase of temperature well beyond midday.

### 6.2. Experimental verification of the mathematical model

Fig. 14 shows the comparison between the measured temperature and the simulated temperature obtained in mid winter.

The maximum absolute error between the simulated and experimental results is  $0.5730^\circ\text{C}$ . Climatic boundary conditions of the weather data from experimental measurements are used for the simulation. A time step of 10 seconds is taken and the final time of the simulation is 672 hours 100 mesh grids are considered. We observe that the calculated and measured data from these periods follow the same trend, except for a few anomalies. These anomalies may arise from experimental errors that occurred while taking measurements or from errors in the sensors used. Next, a comparison between the calculated and measured indoor surface temperature of a cell with green roof in late winter is presented for the period of 10 September to 07 October.

In late winter, it is noted from Fig. 15 that the values obtained by modelling follow almost the same trend as the experimental data. A maximum absolute error of about  $0.7866^\circ\text{C}$  is observed.

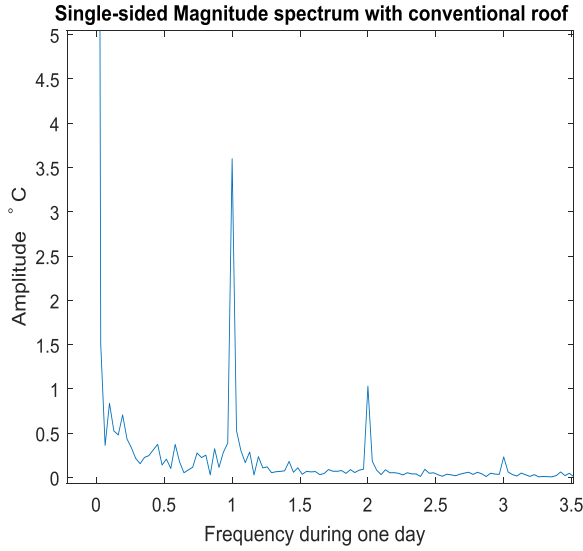
#### 6.2.1. Order of accuracy

Furthermore, a grid refinement study is conducted in order to investigate the accuracy of the implicit FDM. 4 mesh grids are considered whereby the coarsest grid has  $N = 2419200$  temporal nodes and  $J = 100$  spatial nodes. The grids are refined by a factor of 2 on both axes. That is,  $iN = 2419200 \times 2i$  and  $ij = 100 \times 2i$  for the  $i^{\text{th}}$  fine grid. The rate of convergence of the FDM can be calculated from the root mean square error (RMSE)

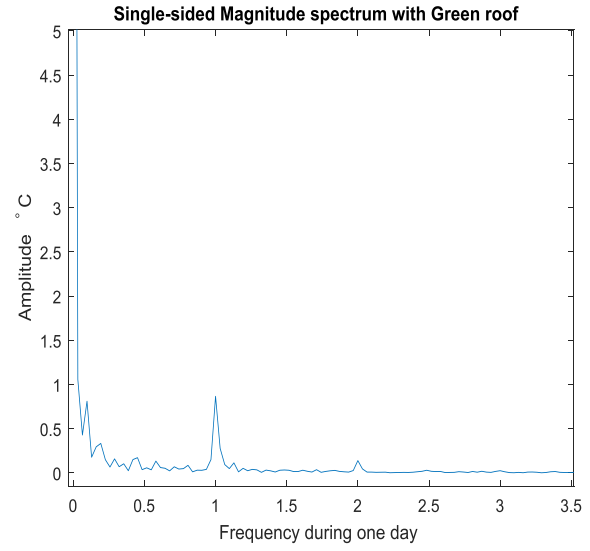
$$E_i = \frac{1}{100} \sqrt{\sum_{j=1}^{100} (T_j^i - T_{2j}^{i+1})^2} \text{ for } i = 1, 2, 3$$

between the coarse and fine solutions [40]. From Fig. 16, the RMSE is seen to decrease on refining the mesh.

Also, the order of accuracy of the scheme is given by



(a) Conventional roof.



(b) Green roof.

Fig. 13. Distribution of peaks in daily temperature.

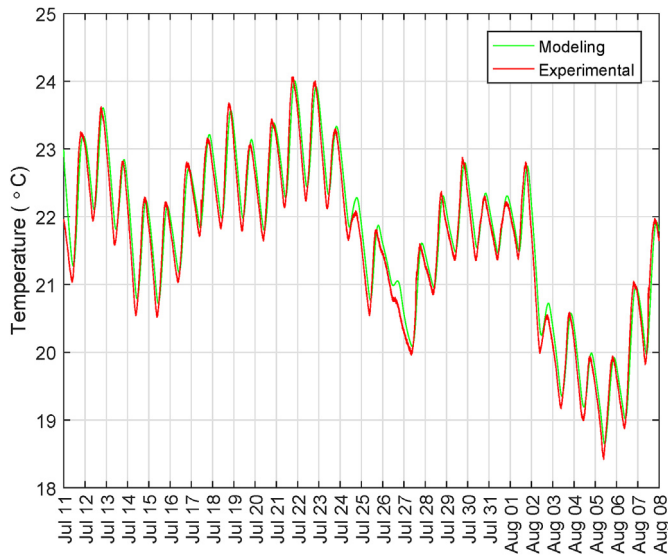


Fig. 14. Experimental and numerical comparison of the temperature inside the cell with green roof in mid winter. (For interpretation of the references to colour in this figure legend, the reader is referred to the Web version of this article.)

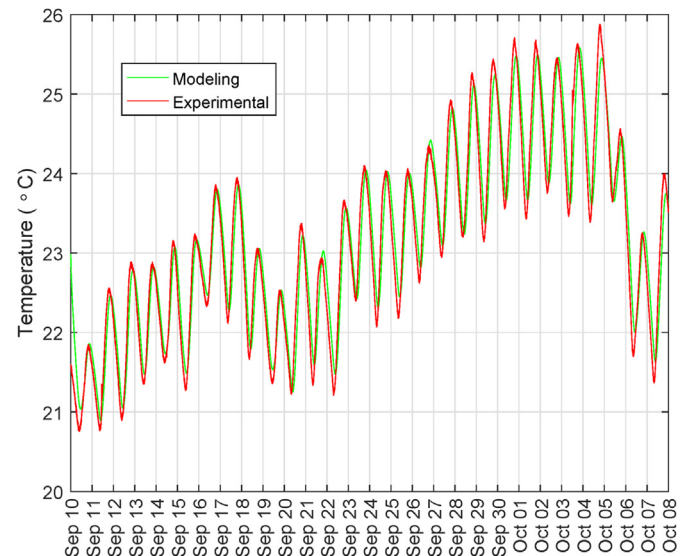


Fig. 15. Experimental and numerical comparison of the temperature inside the cell with green roof in late winter. (For interpretation of the references to colour in this figure legend, the reader is referred to the Web version of this article.)

$$\frac{\log\left(\frac{E_i}{E_{i+1}}\right)}{\log(2)}$$

$(\log(E_1/E_2))/\log(2) = 1.8116$  and  $(\log(E_2/E_3))/\log(2) = 1.7248$  suggest a second order accurate FDM. Also, the accuracy of the implicit FDM can be gauged through the mean bias error (MBE) and cumulative variation of the root mean square error (CV(RMSE)) between the experimental and simulated data [30]. These error measures can be obtained from the following equations:

$$MBE = \frac{\sum_{n=1}^N (E_n - S_n)}{\sum_{n=1}^N E_n} \quad (30)$$

and

$$CV(RMSE) = \frac{\sqrt{\frac{\sum_{n=1}^N (E_n - S_n)^2}{N}}}{\sum_{n=1}^N E_n} \quad (31)$$

where  $E_n$  and  $S_n$  are the experimental and simulated data at an instance in time  $n$ . The MBE shows how accurately the simulated values fit the experimental data, and the CV(RMSE) indicates the overall uncertainty in the predicted results.

From Table 3, the negative values for the MBE suggest that the simulation results over predict the experimental data, and a low positive CV(RMSE) indicates that the data obtained from the mathematical model are close to the corresponding experimental

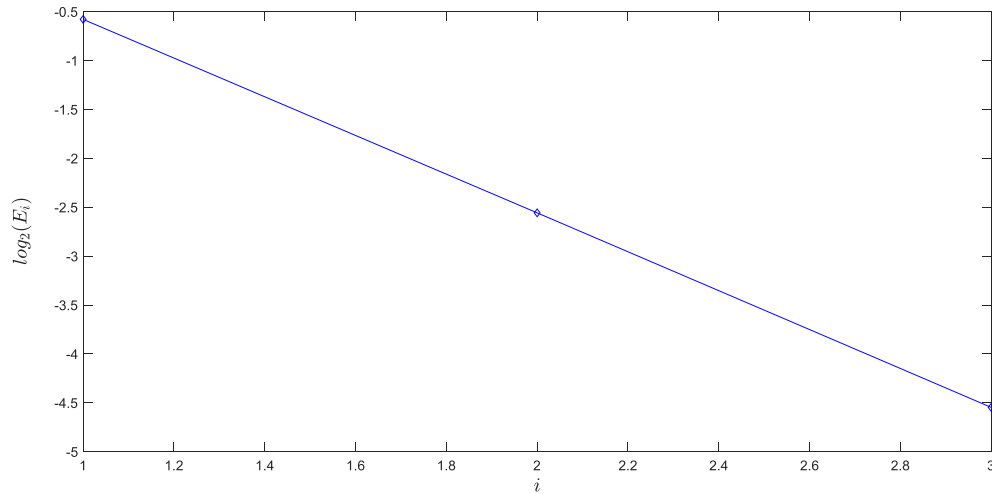


Fig. 16. Root mean square error of the FDM with grid refinement.

Table 3

MBE and CV(RMSE) of the temperature distribution with the green roof model in mid winter and late winter.

	MBE	CV(RMSE)
Mid winter	$-2.7385 \times 10^{-4}$	0.0022
Late winter	$-4.6345 \times 10^{-5}$	0.0023

values. Both error measures are lower than 1%. The discrepancy may be a result of measurement errors. Nevertheless, the numerical method adopted provides sufficient accuracy in order to predict the temperature distribution in the green roof.

### 6.3. Thermal performance of green roof

#### 6.3.1. Comparison of heat flux between green roof and conventional roof

Conductive heat flux is an important parameter which influences thermal performance inside a building. The conductive heat flux is used as an indicator of the transfer of heat energy into or out of a building. A positive heat flux represents heat gained while a negative heat flux represents heat lost. A conductive heat flux of low magnitude means that less heat is moving across the layers. To analyse the thermal performance of the green roof, we calculate the internal surface heat flux,  $q_{int}$ , for green roof and conventional roof as follows

$$q_{int} = -\lambda_c \frac{\partial T}{\partial x} \quad (32)$$

where  $\lambda_c$  is the thermal conductivity of the concrete layer.

From Figs. 17 and 18, it is observed that the internal surface heat flux of a cell with green roof is lower than that of a cell with conventional roof in both mid winter and late winter. The maximum internal surface heat flux on each day for a conventional roof lies between  $30W/m^2$  and  $75W/m^2$  whereas for green roof the internal surface heat flux lies between  $1.5W/m^2$  and  $8W/m^2$ . The green roof acts as an insulation layer by decreasing the room's heat gained thereby reducing the room's cooling demand.

The mathematical formulation of the one dimensional green roof model allows us to calculate and compare the conductive heat transfer arising in both conventional roofs and green roofs. Since the temperature is not uniformly distributed over the roof, the

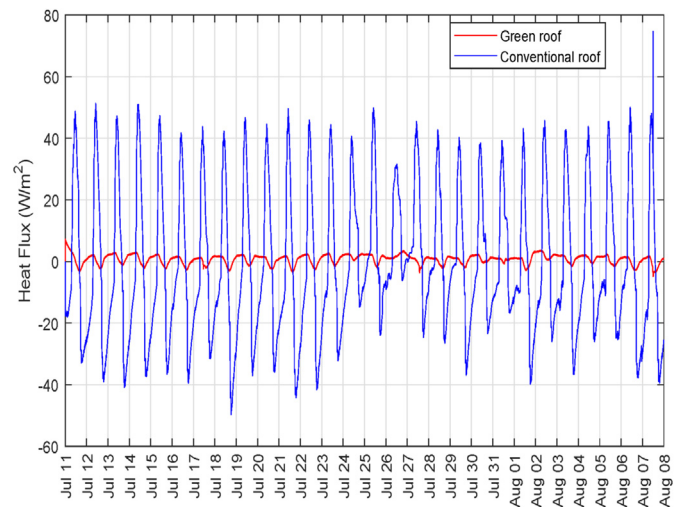


Fig. 17. Internal surface heat flux for green roof and conventional roof in mid winter. (For interpretation of the references to colour in this figure legend, the reader is referred to the Web version of this article.)

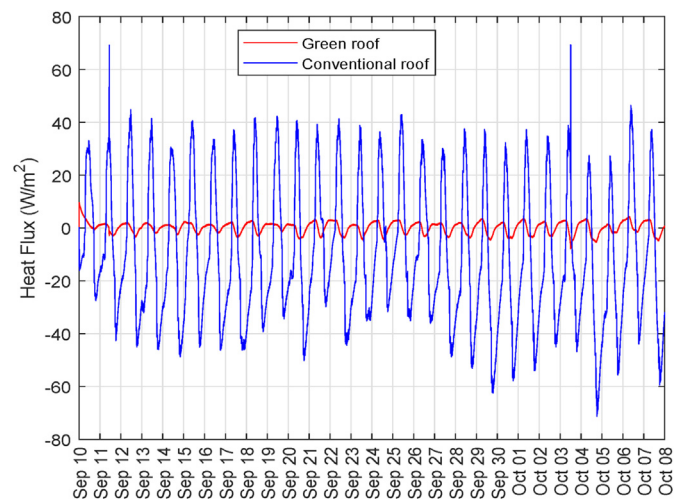


Fig. 18. Internal surface heat flux for green roof and conventional roof in late winter. (For interpretation of the references to colour in this figure legend, the reader is referred to the Web version of this article.)

conductive heat transfer is sought after every  $\Delta x$  and summed over the whole computational domain. The total conductive heat transfer,  $q^T$ , for the multilayer green roof model is calculated as

$$q^T = q^1 + q^2 + q^3 + q^4, \tag{33}$$

where  $q^1$  is the conductive heat transfer for planting layer,  $q^2$  is the conductive heat transfer for substrate layer,  $q^3$  is the conductive heat transfer for waterproofing layer and  $q^4$  is the conductive heat transfer for concrete layer as shown in Fig. 19.

The conductive heat transfer for each layer of the green roof system is calculated as

$$q^k = - \sum_j^{N_k} j = 1 \lambda_k \Delta T_j^k \text{ for } k = 1, 2, 3, 4. \tag{34}$$

where  $\Delta T_j^k = T_{j+1}^k - T_j^k$  and  $\Delta x_j^k = x_{j+1}^k - x_j^k$ .  $T_j^k$  denotes the temperature at the  $j^{\text{th}}$  node in the computational domain of the  $k^{\text{th}}$  layer and  $N_k$  denotes the total number of computational nodes in the  $k^{\text{th}}$  layer. Figs. 20 and 21 show the conductive heat transfer in mid winter and late winter conditions when using a conventional roof and green roof.

From Figs. 20 and 21, it is observed that the conductive heat flux of a conventional roof varies greatly as compared to a green roof. The maximum conductive heat flux on each day for a conventional roof varies from  $0.4797 \text{ W/m}^2$  to  $2.5190 \text{ W/m}^2$  whereas for the

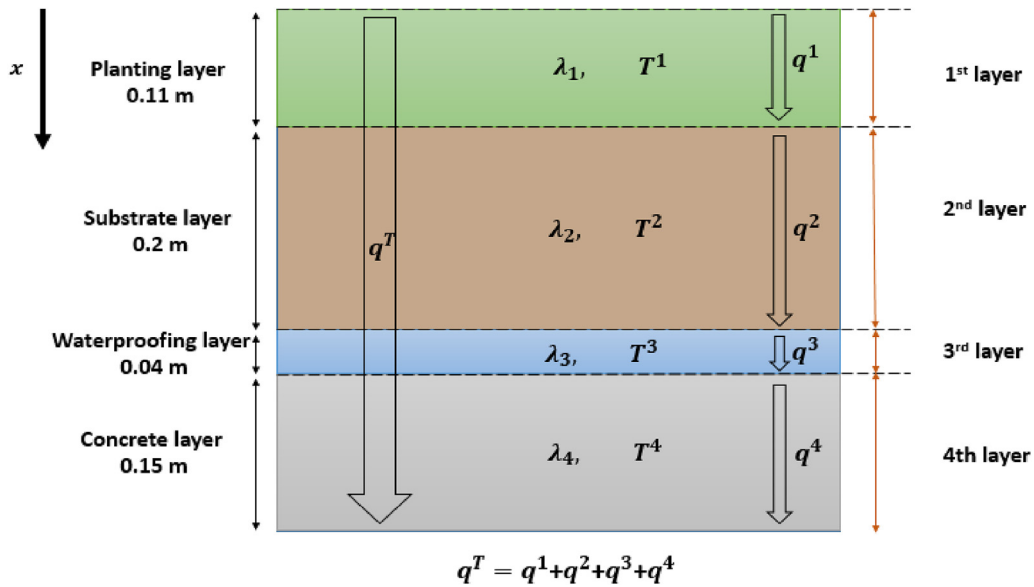


Fig. 19. Schematic representation of the heat transfer within the green roof. (For interpretation of the references to colour in this figure legend, the reader is referred to the Web version of this article.)

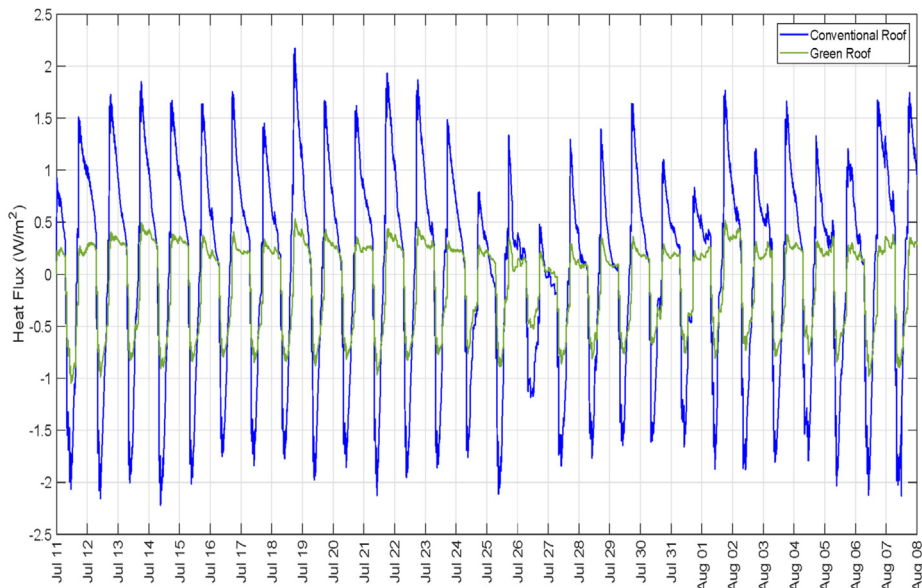


Fig. 20. Conductive heat transfer in mid winter.

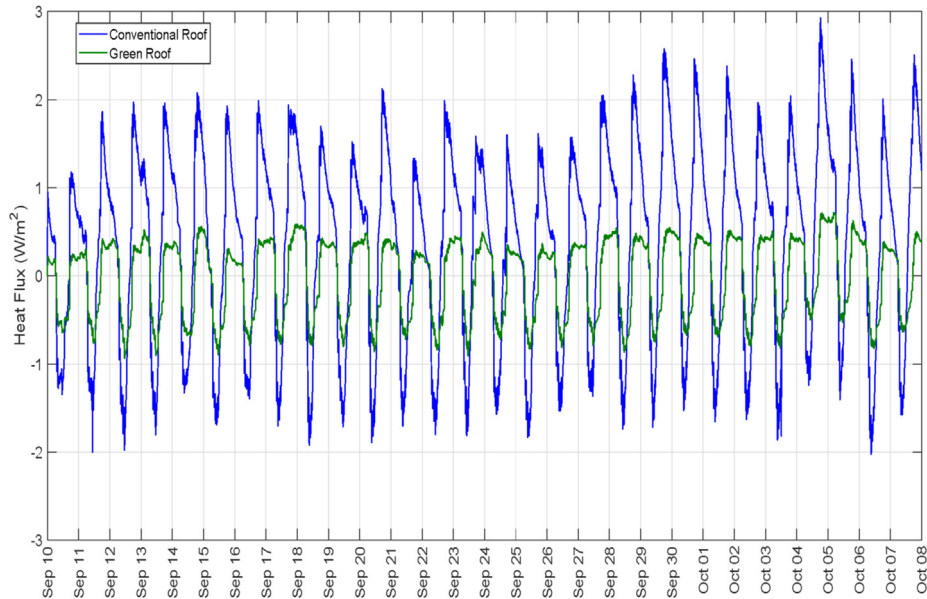


Fig. 21. Conductive heat transfer in late winter.

green roof, it varies from  $0.2090 \text{ W/m}^2$  to  $0.5312 \text{ W/m}^2$ . Overall, it is noted that both in mid winter and late winter, the green roof consistently decreases heat gained when compared to a conventional roof. This can be explained by the fact that green roofs decrease heat entering the roof during the day and release the accumulated heat at night.

6.3.2. Comparison of the thermal performance of a green roof and that of a conventional roof on a sunny and rainy day

Internal air temperature enables us to estimate the thermal behaviour and performance of an indoor environment. From Fig. 11, it is noted that with a conventional roof, the concrete suffers from a large variation in temperature which is from  $16^\circ\text{C}$  to  $32^\circ\text{C}$  whereas with a green roof, there is a small variation in the temperature from  $19^\circ\text{C}$  to  $23^\circ\text{C}$ . The higher temperature on the surface will lead to an increase in internal air temperature. Next, we compare the indoor surface temperature on a sunny day with a green roof cell and a conventional roof cell. Fig. 22 shows the corresponding variation of the temperature inside the cell and Fig. 23

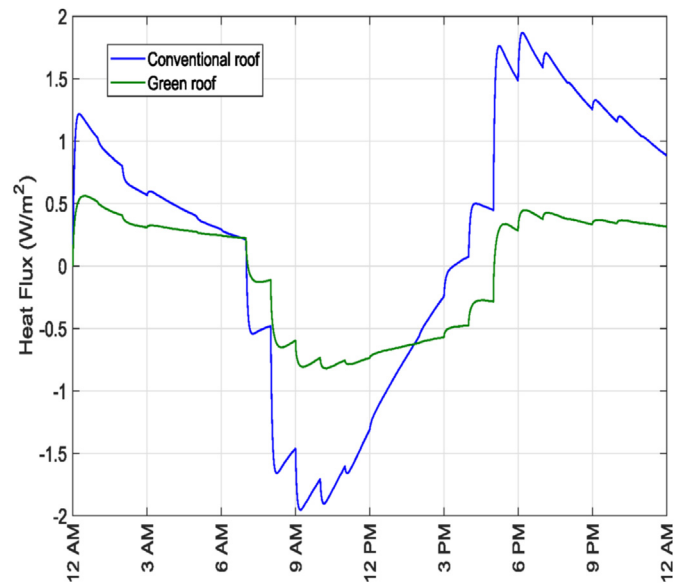


Fig. 23. Corresponding variation of conductive heat flux on a sunny day.

Sunny Day 22-23 July to compare ambient temp, inside temp with green roof and convention

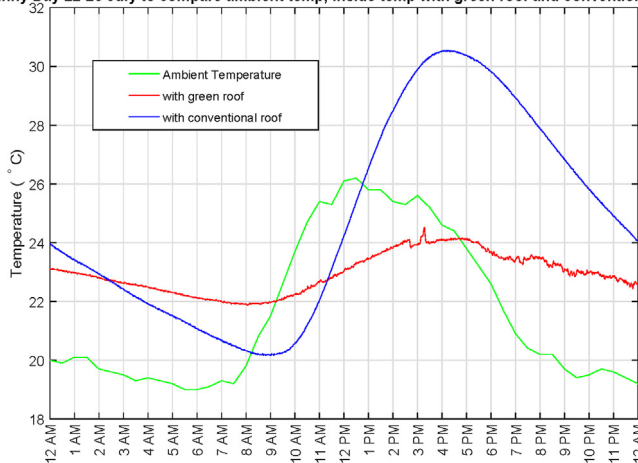


Fig. 22. Indoor surface temperature for green roof and conventional roof respectively on a sunny day. (For interpretation of the references to colour in this figure legend, the reader is referred to the Web version of this article.)

shows the variation of conductive heat flux.

It is observed that the range of variation of the temperature inside a cell with substrate is lower than that of a cell with no substrate. Particularly, a large fluctuation in temperature from  $20^\circ\text{C}$  to  $31^\circ\text{C}$  is observed for the indoor surface temperature of a cell with conventional roof. Also, it is noted that the fluctuation is reduced considerably in a cell with green roof. For the latter cell, the variation in temperature is from  $22^\circ\text{C}$  to  $24^\circ\text{C}$ . Moreover, it should be pointed out that after a sunny day, the inside temperature of a green roof cell at night is higher than that of a conventional roof, but at daytime the cell with green roof is cooler than the cell without green roof.

Fig. 22 shows that the afternoon peak temperature of the conventional roof occurs at around 16:00 whereas that of the green roof is at 17:00. Thus, in addition to attenuate the peak temperature, the green roof delays its occurrence, thereby keeping the indoor conditions comfortable. From these observations, it can be accentuated that the green roof increases the thermal mass of the

material which reduces the fluctuations. Thus, the cooling and heating up occurs at a slower pace for the green roof cell.

This mechanism can be explained by the decrement factor which accounts for the fact that the heat transferred to the outer surface of a building material is partly stored and partly transferred to the indoor space (The decrement factor of the green roof is approximately 0.9 meaning that a variation of 1 °C of the outside temperature will bring a variation of 0.9 °C in the inside temperature of the green roof). Therefore, if the temperature of the wall exceeds the outdoor temperature, then a part of the energy stored is transferred to the outside and not to the indoor space. This is why the temperature starts decreasing for the conventional roof. A similar trend is seen in the case of the green roof but the decrement factor [41] over here has been attenuated because the retaining power capacity of the material has been decreased. As a result, the material does not emit much heat.

Next, we compare the indoor surface temperature effect on a rainy day for the green roof and conventional roof. Fig. 24 shows the variation of the indoor surface temperature of cell with green roof and one with conventional roof during a rainy day at Reduit. The variation of conductive heat flux is given in Fig. 25.

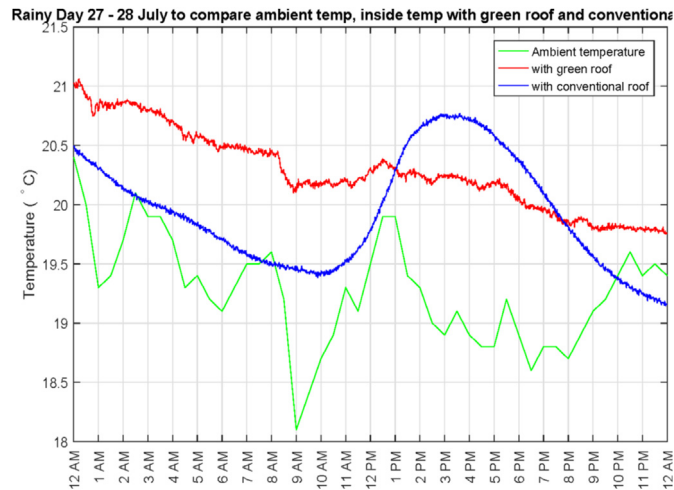


Fig. 24. Indoor surface temperature for green roof and conventional roof on a rainy day. (For interpretation of the references to colour in this figure legend, the reader is referred to the Web version of this article.)

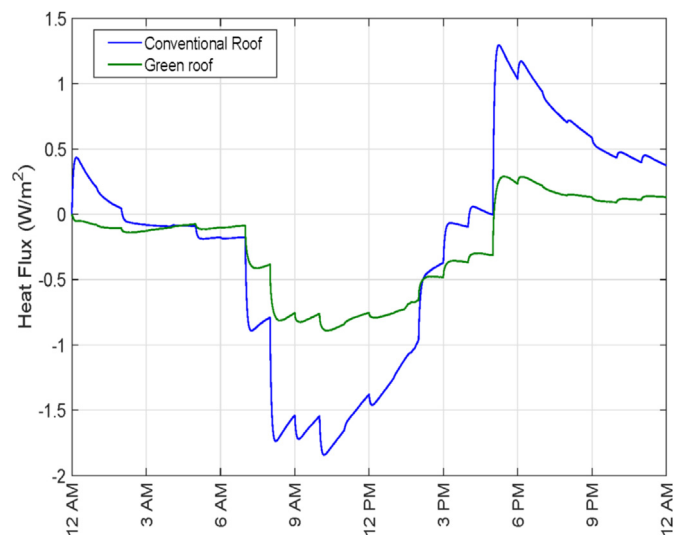


Fig. 25. Corresponding variation of conductive heat flux on a rainy day.

On 27–28 July, the variation of the temperature inside the cell with green roof is lower than the cell with conventional roof despite that it was a rainy day. The inside temperature of a cell with green roof varies between 19.8 °C to 21 °C whereas in a cell with conventional roof, the temperature range is between 19 °C to 21 °C. It is observed that the lower bound of the temperature inside the green roof is higher than the ambient temperature which ranges between 18 °C to 20 °C. This suggests that green roofs increase the thermal performance during both sunny and rainy days.

From Figs. 22 and 23, it can be observed that the peak inside temperature is reached, for both green roof and conventional cell. The corresponding conductive heat flux rate is negative, that is, heat ‘travels’ in the outward direction so that the temperature of each cell decreases accordingly. Since the decrement factor has been reduced in the case of the green roof, the temperature gradient is lower and in this sense, the green roof stabilises the temperature inside. In addition, the layers are dynamically absorbing and regulating moisture, thus adjusting the temperature.

Fig. 26a and b shows the power spectrum of the conductive heat flux data obtained from eq (33) for the conventional roof and green roof respectively.

The same trend is observed as in the power spectrum of the temperature data of both conventional roof and green roof.

### 7. Conclusion

This study investigated the thermal performance of a green roof during mid winter and late winter, under the climatic conditions of Mauritius, which is influenced by a tropical humid climate by using onsite measurements of weather data and indoor temperature. Analysis of the collected data showed that the green roof: (i) increases the thermal mass of the experimental cells under consideration, (ii) damps the heat flux variation (iii) attenuates the two peaks in daily indoor temperature and delays the afternoon peak (iv) the heat flux of a conventional roof varied greatly as compared to that of a green roof. The maximum heat flux on each day for a conventional roof varied from 0.4797W/m<sup>2</sup> to 2.5190W/m<sup>2</sup> whereas for the green roof, it varied from 0.2090W/m<sup>2</sup> to 0.5312W/m<sup>2</sup>. Overall, it was observed that both in mid winter and late winter, the green roof consistently decreased heat gained when compared to a conventional roof. A one dimensional mathematical model was proposed in order to simulate the evolution of the heat and moisture transfer in a porous multilayer material. The numerical results showed that the model simulated the variation of the indoor temperature round the clock quite accurately during the second half of the winter season in Mauritius. The model has the ability to be easily integrated in decision support tools with the capacity of the physically based simulation model to be easily transferred in conditions and locations other than those used for in the present study. Based on the results of this preliminary experimental study and numerical simulations, it can be inferred that a green roof can be an effective alternative in cooling existing buildings with poor roof thermal insulation in Mauritius and eventually reduce electricity consumption due to air conditioning. One of the limitations of the present work is that the experimental system does not have external windows and is not a typical civil building. Further, the cells in the system are quite small to be utilized in the real world. In a future work, a real building model can be selected for further simulations and analyses can be conducted so as to investigate how factors such as the thickness and the thermal conductivity of a given substrate, the leaf area index, leaf emissivity, and the solar absorptivity of the substrate impact green roof performance in the context of the Mauritian climate. In a real building model with green roof, the heat emanating from the left

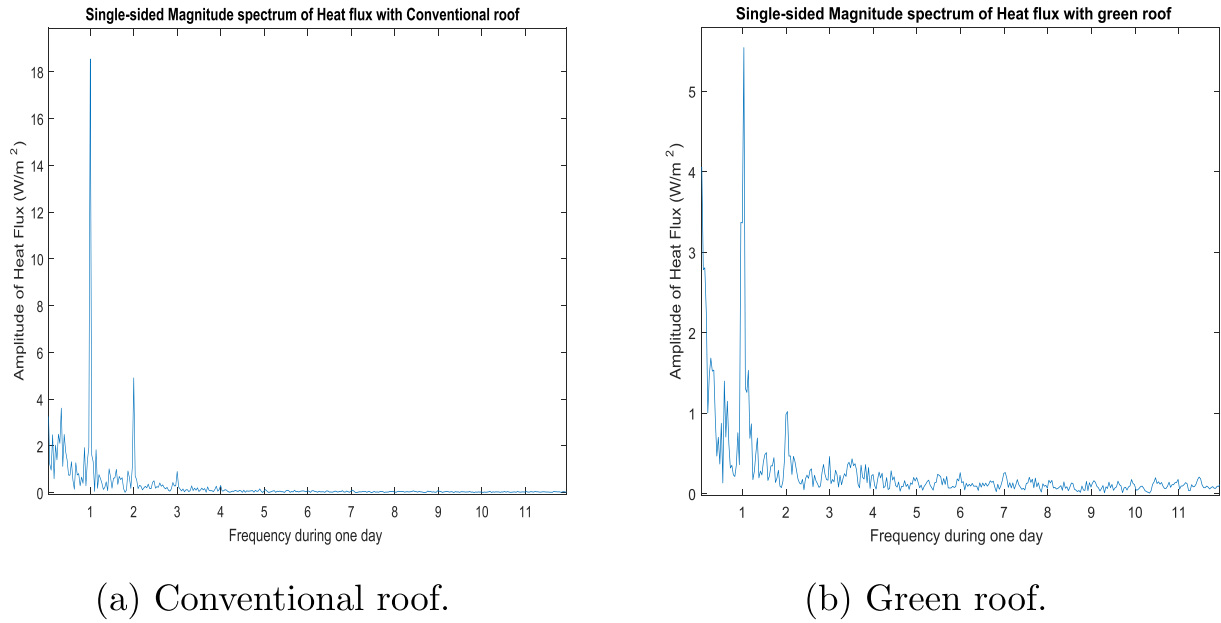


Fig. 26. Distribution of peaks in daily conductive heat flux.

and right vertical walls can be regulated by attenuating the decrement factor of the walls. An effective way of reducing the decrement factor is to consider the growth of lianas and climbing plants on the vertical walls.

**Declaration of competing interest**

The authors declare that they have no known competing financial interests or personal relationships that could have appeared to influence the work reported in this paper.

**CRedit authorship contribution statement**

**Maheshsingh Mungur:** Conceptualization, Formal analysis, Investigation, Writing - original draft. **Yashna Poorun:** Methodology, Software, Validation. **Diksha Juggurnath:** Conceptualization, Data curation. **Yusra Bibi Ruhomally:** Writing - review & editing, Conceptualization. **Reshma Rughooputh:** Investigation, Resources, Project administration. **Muhammad Zaid Dauhoo:** Supervision, Conceptualization, Formal analysis, Writing - review & editing. **Abdel Khodaruth:** Resources, Data curation. **Heman Shamachurn:** Investigation, Resources. **Mahendra Gooroochurn:** Investigation, Resources. **Navindra Boodia:** Resources. **Mahindra Chooneea:** Resources. **Sunita Facknath:** Funding acquisition, Project administration.

**Acknowledgements**

The research was supported by the Mauritius Research and Innovation Council (MRC) (Grant number: MRC/RUN/1719). We thank the United Basalt Products Ltd. (UBP) for sponsoring this research. The authors would like to kindly acknowledge the referees for their constructive comments and recommendations for the present article.

**Appendix**

*Theorem @.1*

The system of equations (13) - (14) is well-posed if  $D_h \left( \frac{dT}{dH} \right) \left( \lambda \frac{dh}{dw} + h_v \delta_p A \right) > \left[ \frac{\delta_p}{2} (A - B) \right]^2$ , where  $A = h \frac{dh}{dw} \frac{dP_{sat}}{dT}$  and  $B = h_v P_{sat} \frac{dT}{dH}$ .

Proof Eq (13) and Eq (14) can be written as:

$$\frac{\partial}{\partial t} \Phi = C \frac{\partial^2}{\partial x^2} \Phi, \tag{35}$$

where  $\Phi = \left( \frac{h}{T} \right)$  and

$$C = \begin{pmatrix} \frac{dh}{dw} (D_h + \delta_p P_{sat}) & \frac{dh}{dw} \left( \delta_p h \frac{dP_{sat}}{dT} \right) \\ \frac{dH}{dT} (h_v \delta_p P_{sat}) & \frac{dT}{dH} \left( \lambda + h_v \delta_p h \frac{dP_{sat}}{dT} \right) \end{pmatrix}. \text{ For the system to be well-posed, } C_{sys} \text{ which is given by:}$$

$$C_{sys} = \frac{1}{2} (C + C^T) = \begin{pmatrix} \frac{dh}{dw} (D_h + \delta_p P_{sat}) & \frac{1}{2} \left( \frac{dh}{dw} \left( \delta_p h \frac{dP_{sat}}{dT} \right) + \frac{dH}{dT} (h_v \delta_p P_{sat}) \right) \\ \frac{1}{2} \left( \frac{dh}{dw} \left( \delta_p h \frac{dP_{sat}}{dT} \right) + \frac{dH}{dT} (h_v \delta_p P_{sat}) \right) & \frac{dT}{dH} \left( \lambda + h_v \delta_p h \frac{dP_{sat}}{dT} \right) \end{pmatrix}, \tag{36}$$

must be positive definite [42], where the superscript  $T$  represents the matrix transpose. The principal minors of matrix  $C_{sys}$  are given by

$$M_1 = \frac{dh}{dw} (D_h + \delta_p P_{sat}) \quad (@.37)$$

and

$$M_2 = \frac{dh}{dw} \frac{dT}{dH} (D_h + \delta_p P_{sat}) \left( \lambda + h_v \delta_p h \frac{dP_{sat}}{dT} \right) - \frac{1}{4} \left[ \frac{dh}{dw} \left( \delta_p h \frac{dP_{sat}}{dT} \right) + \frac{dT}{dH} (h_v \delta_p P_{sat}) \right]^2 \quad (@.38)$$

Since  $\frac{dh}{dw} > 0$ ,  $D_h > 0$ ,  $\delta_p > 0$  and  $P_{sat} > 0$ , we get  $M_1 > 0$ .

$$\text{Now, } M_2 > 0 \Leftrightarrow D_h \left( \frac{dT}{dH} \right) \left( \lambda \frac{dh}{dw} + h_v \delta_p A \right) > \left[ \frac{\delta_p}{2} (A - B) \right]^2, \quad (@.39)$$

where  $A = h \left( \frac{dh}{dw} \right) \left( \frac{dP_{sat}}{dT} \right)$  and  $B = h_v P_{sat} \left( \frac{dT}{dH} \right)$ . Since the principal minors  $M_1$  and  $M_2$  are positive, by Sylvester's law the assertion in Theorem @.1 holds.

## Nomenclature

$a$	Short wave radiation absorptivity coefficients
$a_r$	Precipitation absorptivity
$c_e$	Specific heat capacity of ice (J/kgK)
$c_s$	Specific heat capacity (J/(kgK))
$c_w$	Specific heat capacity of liquid water (J/kgK)
$D_h$	Liquid conduction coefficient (kg/(ms))
$g_l$	Liquid flux (kg/m <sup>2</sup> s)
$g_v$	Vapour flux (kg/m <sup>2</sup> s)
$h$	Relative humidity
$h_v$	Latent heat of phase change (J/kg)
$h_e$	Specific melting enthalpy (J/kg)
$H$	Total enthalpy (J/m <sup>3</sup> )
$H_s$	Enthalpy of dry material (J/m <sup>3</sup> )
$H_w$	Enthalpy of the moist material (J/m <sup>3</sup> )
$I$	Net radiation (W/m <sup>2</sup> )
$I_e$	Long wave emission
$I_l$	Long wave radiation
$I_s$	Incoming solar radiation
$P$	Porosity (m <sup>3</sup> /m <sup>3</sup> )
$p_a$	Water vapour pressure at the ambient temperature (Pa)
$p_c$	Water vapour pressure at the canopy (Pa)
$p_{c,sat}$	Related saturation pressure (Pa)
$p_v$	Vapour partial pressure (Pa)
$q$	Heat flux (W/m <sup>2</sup> )
$q_i^C$	Heat conduction flux for the $i^{th}$ layer (W/m <sup>2</sup> )
$q_{ext}$	Exterior heat flux (W/m <sup>2</sup> )
$R$	Universal gas constant
$R_N$	Normal rain (kg/(m <sup>2</sup> s))
$R_s$	Driving rain (kg/(m <sup>2</sup> s))
$r_s$	Driving rain coefficient (s/m)
$S_h$	Heat source/sink (W/m <sup>3</sup> )
$S_w$	Moisture source/sink (kg/(m <sup>3</sup> s))
$T$	Temperature (K)
$T_c$	Canopy temperature (K)
$T_a$	Ambient temperature (K)
$T_s$	Surface temperature (K)
$T^*$	Equivalent exterior temperature (K)

$t$	Time
$v$	Wind velocity (m/s)
$w$	Water content of the material layer (kg/m <sup>3</sup> )
$w_e$	Content of frozen water (kg/m <sup>3</sup> )
$\rho_B$	Bulk density (kg/m <sup>3</sup> )
$\frac{dH}{dT}$	Heat storage capacity (J/(m <sup>3</sup> K))
$\frac{dw}{dh}$	Moisture storage capacity (kg/m <sup>3</sup> )
$\frac{dP_{sat}}{dT}$	Slope of water vapour saturation pressure curve

## Greek symbols

$\alpha$	Heat transfer coefficient (W/m <sup>2</sup> K)
$\alpha_c$	Convective heat transfer coefficient (W/m <sup>2</sup> K)
$\alpha_r$	Radiative heat transfer coefficient (W/m <sup>2</sup> K)
$\beta$	Water vapour transfer coefficient (kg/(m <sup>2</sup> sPa))
$\epsilon$	Surface emissivity
$\sigma$	Stefan Boltzmann constant (W/(m <sup>2</sup> K <sup>4</sup> ))
$\lambda$	Thermal conductivity (W/(mK))
$\mu$	Vapour diffusion factor
$\delta_p$	Water vapour permeability (kg/(msPa))

## Subscripts

$c$	Canopy
$s$	Surface
$a$	Ambient

## Superscripts

$C$	Conduction
$*$	Equivalent exterior

## References

- [1] Berndtsson JC, Bengtsson L, Jinno K. Runoff water quality from intensive and extensive vegetated roofs. *Ecol Eng* 2009;35(3):369–80.
- [2] Fioretti R, Palla A, Lanza L, Principi P. Green roof energy and water related performance in the mediterranean climate. *Build Environ* 2010;45(8):1890–904.
- [3] Lazzarin RM, Castellotti F, Busato F. Experimental measurements and numerical modelling of a green roof. *Energy Build* 2005;37(12):1260–7.
- [4] MacIvor JS, Lundholm J. Performance evaluation of native plants suited to extensive green roof conditions in a maritime climate. *Ecol Eng* 2011;37(3):407–17.
- [5] Del Barrio EP. Roof components models simplification via statistical linearisation and model reduction techniques. *Energy Build* 1999;29(3):259–81.
- [6] Wong NH, Cheong DW, Yan H, Soh J, Ong C, Sia A. The effects of rooftop garden on energy consumption of a commercial building in Singapore. *Energy Build* 2003;35(4):353–64.
- [7] Dominique M, Tiana RH, Fanomezana RT, Ludovic AA. Thermal behavior of green roof in reunion island: contribution towards a net zero building. *Energy Procedia* 2014;57:1908–21.
- [8] Peng Z, Smith C, Stovin V. Internal fluctuations in green roof substrate moisture content during storm events: monitored data and model simulations. *J Hydrol* 2019;573:872–84.
- [9] Yin H, Kong F, Dronova I, Middel A, James P. Investigation of extensive green roof outdoor spatio-temporal thermal performance during summer in a subtropical monsoon climate. *Sci Total Environ* 2019;696:133976.
- [10] Quezada-García S, Espinosa-Paredes G, Escobedo-Izquierdo M, Vázquez-Rodríguez A, Vázquez-Rodríguez R, Ambríz-García J. Heterogeneous model for heat transfer in green roof systems. *Energy and Buildings*; 2017.
- [11] Ouldoukhitine S-E, Belarbi R, Jaffal I, Trabelsi A. Assessment of green roof thermal behavior: a coupled heat and mass transfer model. *Build Environ* 2011;46(12):2624–31.
- [12] Rakotondramiarana HT, Ranaivoarisoa TF, Morau D. Dynamic simulation of the green roofs impact on building energy performance, case study of antananarivo, Madagascar. *Buildings* 2015;5(2):497–520.
- [13] Sailor DJ. A green roof model for building energy simulation programs. *Energy Build* 2008;40(8):1466–78.
- [14] Yang J, Pyrgou A, Chong A, Santamouris M, Kolokotsa D, Lee SE, et al. Green and cool roofs urban heat island mitigation potential in tropical climate. *Sol Energy* 2018;173:597–609.
- [15] Liu X, Chui TFM. Evaluation of green roof performance in mitigating the impact of extreme storms. *Water* 2019;11(4): 815.
- [16] Baryła A, Gnatowski T, Karczmarczyk A, Szatyłowicz J. Changes in temperature and moisture content of an extensive-type green roof. *Sustainability*

- 2019;11(9). 2498.
- [17] Zhou L, Wang Q, Li Y, Liu M, Wang R. Green roof simulation with a seasonally variable leaf area index. *Energy Build* 2018;174:156–67.
- [18] M. Akther, J. He, A. Chu, J. Huang, and B. van Duin, "A review of green roof applications for managing urban stormwater in different climatic zones," *Sustainability*, vol. 10, no. 8 (2864), 2018.
- [19] Quezada-García S, Escobedo-Izquierdo MA, Ambriz-García JJ, Vázquez-Rodríguez R, Morales-Ramírez D. Comparison of green roof model predictions with experimental data. *Energy Res J* 2015;6(1):15.
- [20] Jim CY. Air-conditioning energy consumption due to green roofs with different building thermal insulation. *Appl Energy* 2014;128:49–59.
- [21] Doshi H, Banting D, Li J, Missios P, Au A, Currie B, Verrati M. Environmental benefits of green roofs on a city scalean example of city of toronto. In *proc. Of 4th north American green roof conference*. Boston: Greening Rooftops for Sustainable Communities; 2006.
- [22] Ascione F, Bianco N, deRossi F, Turni G, Vanoli GP. Green roofs in european climates. are effective solutions for the energy savings in air-conditioning? *Appl Energy* 2013;104:845–59.
- [23] Leonard T, Leonard J. The green roof and energy performance: rooftop data analyzed. In: *Proceedings of the 3rd north American green roof conference: greening rooftops for sustainable communities*. Washington, DC. Toronto: The Cardinal Group; 2005.
- [24] Defimedia. website, URL:<https://defimedia.info/hausse-de-la-consommation-deelectricite-en-ete-les-factures-de-janvier-et-fevrier-2020-risquent-detre-plus-elevees-previent?fbclid=IwAR1btnCF35z5LNa-iewA-CoW071mj5Vi7d46f9aDd5Xf3174HgZrcCWz0zI>, . [Accessed 21 December 2019].
- [25] Elahee M. Energy management and air-conditioning in buildings in Mauritius: towards achieving sustainability in a small-island developing economy vulnerable to climate change. *Energy Procedia* 2014;62:629–38.
- [26] Adam NB, Elahee M, Dauhoo M. Forecasting of peak electricity demand in Mauritius using the non- homogeneous gompertz diffusion process. *Energy* 2011;36(12):6763–9.
- [27] Lin B-S, Yu C-C, Su A-T, Lin Y-J. Impact of climatic conditions on the thermal effectiveness of an extensive green roof. *Build Environ* 2013;67:26–33.
- [28] Ahmadi H, Arabi R, Fatahi L. Impact of climatic conditions on the thermal effectiveness of an extensive green roof. *Special Issue of Current World Environment* 2015;10.
- [29] Theodosiou T, Aravantinos D, Tsikaloudaki K. Thermal behaviour of a green vs. a conventional roof under mediterranean climate conditions. *Int J Sustain Energy* 2014;33(1):227–41.
- [30] Zhang Y, Zhang L, Ma L, Meng Q, Ren P. Cooling benefits of an extensive green roof and sensitivity analysis of its parameters in subtropical areas. *Energies* 2019;12(22). 4278.
- [31] Mauritius meteorological services. website, URL:<http://metservice.intnet.mu/climate-services/climate-of-mauritius.php>, . [Accessed 30 December 2019].
- [32] Solar resource maps and gis data. website, URL:<https://solargis.com/maps-and-gis-data/download/mauritius>, . [Accessed 22 December 2019].
- [33] Kunzel HM, et al. Simultaneous heat and moisture transport in building components. Allemagne: *Fraunhofer Institute of building physics*; 1995.
- [34] Janssen H, Blocken B, Roels S, Carmeliet J. Wind-driven rain as a boundary condition for ham simulations: analysis of simplified modelling approaches. *Build Environ* 2007;42(4):1555–67.
- [35] Ak MA, Katoh Y, Katsurayama H, Koganei M, Mizunuma M. Effects of convection heat transfer on sunagoke moss green roof: a laboratory study. *Energy Build* 2018;158:1417–28.
- [36] Ortega-Farias S, Antonioletti R, Oliosio A. Net radiation model evaluation at an hourly time step for mediterranean conditions. 2000.
- [37] Asatutjarit C, Hirunlabh J, Khedari J, Charoenvai S, Zeghamati B, Shin UC. Development of coconut coir-based lightweight cement board. *Construct Build Mater* 2007;21(2):277–88.
- [38] Dvorak BD, Volder A. Plant establishment on unirrigated green roof modules in a subtropical climate. *AoB Plants* 2013;5.
- [39] Cerna M, Harvey AF. The fundamentals of fft-based signal analysis and measurement. *National Instruments* 2000;54. Junho.
- [40] Davie AM, Gaines JG. Convergence of numerical schemes for the solution of parabolic stochastic partial differential equations. *Math Comput* 2001;70(233):121–34.
- [41] Asan H. Numerical computation of time lags and decrement factors for different building materials. *Build Environ* 2006;41(5):615–20.
- [42] Y. Poorun, M. Dauhoo, M. Bessafi, M. Elahee, A. Gopaul, and A. Khoodaruth, "The physical and qualitative analysis of fluctuations in air and vapour concentrations in a porous medium," *Royal Society open science*, vol. 5, no. 5 (171954), 2018.